

Parameter Estimation for Resin Transfer Molding

Vojin Jovanovic Souran Manoochehri Constantin Chassapis
fractal97@hotmail.com, souran@dmi.stevens-tech.edu, costas@dmi.stevens-tech.edu
Design and Manufacturing Institute
Stevens Institute of Technology
Hoboken, NJ, USA

Keywords *Voronoi, weld lines, resin transfer molding, shortest path, polyhedral*

Abstract *A simplified approach for estimating weld lines, vent locations and fill times for resin transfer molding applications in non-planar geometry is presented. The molding parts are treated as polyhedral spaces for which the concept of Voronoi diagram and shortest paths is utilized to predict the formation of weld lines, location of vents and filling times. The approach is based purely on geometrical considerations and on previously established observations that it is possible to treat the resin flow inside the mold as partly radial and partly channel-like. The proposed procedure is geared towards software implementation, but it enables one to gain more insight into the process before detailed and time consuming calculations are attempted.*

1. Introduction

Resin Transfer Molding (RTM) is a versatile polymer composite process for high volume, high performance, and low cost manufacturing. RTM is gaining prominence in almost all areas of the composite industry. In this process a fiber preform of reinforcing material is placed in the mold. The mold is then closed, and a prepolymer is injected which impregnates the fiber preform and fills the heated mold where it cures to create a composite part. RTM owes its popularity to its net shape forming capabilities and the total control the designer has over the orientation of the reinforcing fibers, thus the ability to tailor the properties of the final part to meet the requirements for the desired application.

Due to its significance, several researchers have studied the RTM process with the major emphasis on using the finite element method to determine weld lines of the injected polymer, needed vent locations and filling times. Weld lines, as shown in Figure 1, refer to weaker regions formed by the impingement of two separate flow fronts. Vent locations are the positions that have been filled last which results in air entrapments. These ingredients represent the most important factors to be determined once a mold for a particular part has been designed. For the summary of the available techniques refer to Yalvac et al. (1992), Advani (1994), Antonelli and Farina (1999), Golstanian and El-Gizawy (1998) and Mohan et al.(1999). These techniques usually involve a complicated computer model that can compute fluid flow

analysis using the finite element approach. As such, this kind of analysis requires a long computation time, therefore is a laborious process. Due to the complexity of RTM process analysis, a need arose for some simplified techniques that could in a short amount of time provide main characteristics of the RTM process. As a result a simplified resin flow calculation of the RTM process was proposed in Cai (1992) which gives closed form solutions for some simple thin mold sections with various inlet boundary conditions. The article illustrated some basic concepts that should be used in the mold design and vent arrangement. This effort was further carried to a new level in Biccard et al. (1995) where the researchers investigated a model that predicts proper vent locations and fill time during RTM for general thin 2D sections. The results for some simple geometrical shapes predicted fill times and vent arrangements that agreed well with the experiments. The time required to fill the mold was calculated by treating the resin flow inside the mold as partly radial and partly channel-like.

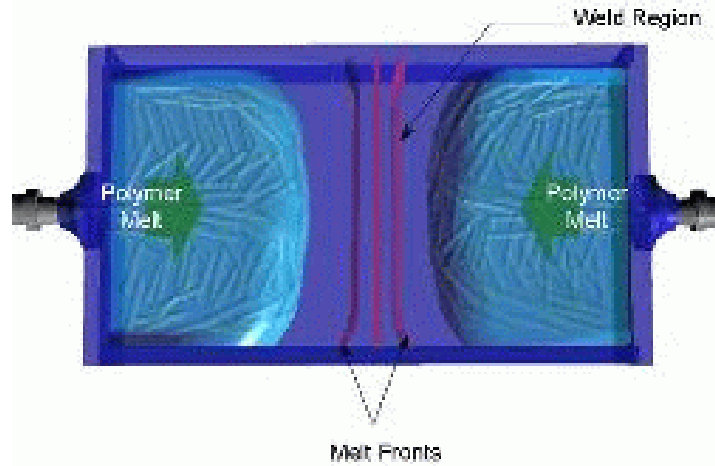


Figure 1. Multigated molds leading to head-on impingement of two separate flow fronts

In this paper, we investigate the possibility of similar treatment to estimate vent locations, weld lines arrangement and filling times for a flat "thin" preform with non-planar geometry whose uniform thickness is small compared to its length and width. We limit our investigation to preforms with isotropic permeability. We will formalize previous attempts with the concept of Voronoi diagrams introduced in computational geometry (Okabe et al, 1992), a widely used tool for solving proximity relations among a set of objects in the plane. Such a treatment together with classical shortest path algorithms from graph theory will enable us to estimate vent locations on bodies approximated by polyhedral shapes or polyhedral surfaces which are topologically equivalent to a disk.

2. RTM Process

The RTM process consists of four phases. The first phase, preform manufacture, consists of assembling of the reinforcement fibers into specified shapes after which the preform is placed into the mold in the appropriate orientation. The second phase, mold filling, starts when the viscous fluid is injected into the hot mold. The fluid flows around and through the fiber network until the mold is filled. Vents should be arranged in such a way to enable air evacuation by the advancing flow front. Ideally they should be placed at the points of the mold which fill last. The third phase, curing, begins near the end of the mold

filling. The curing process is initiated due to the heat transfer from the hot mold to the cold resin where the resin react to form a cross-linked polymer network. This reaction causes the resin to gel and eventually solidify. The curing should not begin until the mold is nearly filled otherwise the dry spots and voids would be formed in the finished part. The final phase, part removal, takes place after the curing reaction is sufficiently complete and the part has solidified.

The mold filling pattern of a fluid through the fiber preform depends on a number of parameters. The most critical are the part geometry, location of the injection gates, injection pressures and flow rates. These parameters have the greatest effect on the final outcome of RTM parts which typically are non-planar shell structures; the thickness being much less than other dimensions of the part. In the manufacturing phase, multiple gates can be used to inject the fluid into the part, and injecting can take place by regulating the flow rate or the injection pressure. To add to the complexity of process modeling, an understanding of the physics on the scale of a fiber diameter is necessary to predict with greater accuracy a priori the relationship between the fiber preform geometry and resistance to flow. Finally the prediction of the location of the flow front during the mold filling phase is most useful in addressing several critical issues. However, this is the one of the most computationally involved problems in RTM.

Our aim is to address the aforementioned issues mainly through geometry and estimate some of the more important parameters in RTM based on mold geometry. Before proceeding further, a brief introduction of the Voronoi diagram is given in the following section.

3. Voronoi Diagram and Resin Flow

The concept of the Voronoi diagram is more than a century old, discussed in 1850 by Dirichlet and in a 1908 paper of Voronoi (Aurenhammer, 1991). The purpose of the diagram is to answer questions about the proximity: who is closest to whom? who is furthest? and so on. A short introduction to the basic concept follows.

Given a set S of n distinct points in \mathfrak{R}^2 (these are called the Voronoi sites), a Voronoi diagram is the partition of \mathfrak{R}^2 into n polygonal regions $vo(p)$ where $p \in S$. Each region $vo(p)$, called the Voronoi cell of p , is defined as the set of points in \mathfrak{R}^2 which are closer to p than to any other points in S , or more precisely,

$$vo(p) = \{x \in \mathfrak{R}^2 : |x - p| \leq |x - q| \forall q \in S - p\} \quad (1)$$

The set of all Voronoi cells forms a cell complex. The vertices of this complex are called the Voronoi vertices, and the extreme rays (i.e. unbounded edges) are the Voronoi rays. A visual representation of the Voronoi diagram is depicted in Figure 2. The Voronoi diagram plays a very important role in computational geometry and for its construction there exist many algorithms which are listed in Okabe et al (1992).

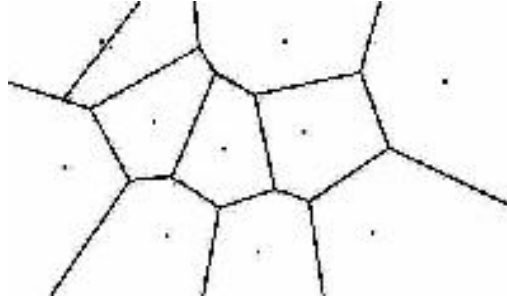


Figure 2. Voronoi diagram in the plane.

To establish the connection between the Voronoi diagram and the resin flow in the plane it is sufficient to associate the inlet ports with Voronoi sites. If the resin is introduced through the points at the same instance, after a certain period of time the region will be completely filled and the weld lines formed will resemble the Voronoi diagram.

In Biccard et al. (1995) a graphical procedure was explained that involves geometrical subdivision of the mold into the subdomains. The proposed procedure actually is a construction of the Voronoi diagram. Once the diagram is constructed, for each Voronoi cell the locations of the vents are determined by plotting the distance r versus s where r is the Euclidian distance between the cell's inlet port and a position s along the cell's perimeter. Vents are then located at the maximum of the r versus s curve. When there are inserts, which are objects that restrict resin flow advancements inside the subdomains, the Euclidian distance r becomes the length of the shortest path. The author's approach shows that the distribution of the liquid in experiments supports the Voronoi model which enables determination of the vent locations to a reasonable degree of accuracy.

The above method was developed using geometrical information only and was based on the assumption that the resin will flow along the shortest possible paths to reach the furthest points of the domain. The shortest paths can be understood as the paths of the minimum potential energy of the flow. The described model is bound to errors due to simplifying of the problem to only a few parameters, nevertheless, it provides reasonable estimates which one can use to decide whether a more accurate numerical analysis should be performed.

4. Shortest Path in Polyhedral Spaces

To generalize the above concept in parts with thin-shell geometry, our aim is to investigate the forming of weld lines in polyhedral spaces. In such cases we need to be able to calculate surface metrics between points that belong to these 2D spaces. In particular we need to find the shortest path along the surfaces between points.

Let P be a finite collection of n planar bounded polygonal faces f_i which is topologically equivalent to a disk. We limit our investigations to polyhedral regions topologically equivalent to a disk, because at this time it is not clear how the Voronoi model can be applied to other topological regions. Let s and p be two points on P . Denote $\pi(s,p)$ to be the shortest path along P from a source s to a point p . The problem is to find the shortest path between s and p which is constrained to lie on P . For detailed characterization of shortest paths on convex polyhedra refer to Sharir and Schorr (1986).

The problem is far from being trivial. In the past decade a few theoretical algorithms have appeared which are mostly concerned with reducing the computational time. The latest one, which is the state of the art in computational time of $O(n^2)$ can be found in Chen and Han (1996). However, from the practical point of view these algorithm are difficult to implement. For this reason we will use a simple approach based on graph theory. With this we do not aspire to compete with other algorithms since our goal is merely to achieve distance calculation for estimation of weld lines in RTM.

In the remaining part of this section we will describe a simple shortest path algorithm in polyhedral spaces. Note that due to graph theory treatment, it is irrelevant whether the polyhedra are convex or nonconvex. Such ignorance is not permissible with other algorithms which further complicates their implementation.

A graph G is an object consisting of two sets called its vertex set V and its edge set E and it is denoted by $G = (V,E)$. The vertex set is a finite non-empty set. The edge set may be empty, but otherwise each element of E is a set $\{v,w\}$ where $v,w \in V$. A good introduction to graphs can be found in Deo (1974). Graphs can be used to represent polyhedral objects where vertices and edges of a graph are associated with vertices and edges of polyhedra respectively as depicted in Figure 3.

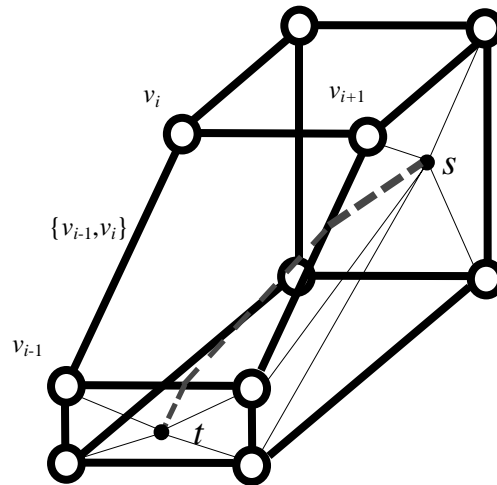


Figure 3. A non-planar depiction of a polyhedron with the shortest path between s and t represented as a dashed line.

A graph may be weighted (where the edges of the graph are associated with positive real numbers) and it may become significant to find the shortest path between the vertices of the graph relative to the weights. Weights may represent the Euclidian distance between vertices. The shortest path between two vertices is the path from all of the possible paths between these two vertices that has the smallest sum of weights. Such a problem arises in the area of network flows, transportation, etc. The problem has had a long and rich history starting with Dijkstra's shortest path algorithm (Dijkstra, 1959) which involves a relatively simple implementation. In our application we will use this algorithm to determine distances on the surface of the polyhedra.

Suppose we are given P which represents a finite collection of connected polygonal faces. First we create a graph G by associating vertices and edges of P with vertices and edges of G , respectively. Also, we associate edges of G with lengths of the corresponding edges of P . Our goal is to find the shortest

path along P between two points that belong to P . Therefore we add to G two new vertices s and t and corresponding edges created by mutually connecting the vertices of the faces where s and t lie as depicted in Figure 3. This is our initial configuration for G . We say initial because a true shortest path on P between s and t will in general cross-section the edges of G and we need to dynamically update G with new vertices while the search for this path is being performed. To this end, the following observation will be useful.

Suppose that at every mid-point of every edge e of G that corresponds to the edge of P we insert a new vertex w . We add these vertices to G and redefine all edges e to incorporate the change. We also add to G all the edges that can be created between all the vertices that lie on P and call it G_1 . We then perform the same procedure recursively starting from G_1 to obtain G_2 and so on. We finally arrive at some G_m in which every original edge of G that corresponds to the edge of P is subdivided into $m + 1$ edges. Now, let $\pi^{G_m}(s,t)$ be the shortest path from s to t in G_m , then, there exists a positive integer N and a real number $\epsilon > 0$ such that $|\pi^{G_m}(s,t) - \pi(s,t)| < \epsilon$ for all $m \geq N$. This statement is based on the fact that G_m will completely cover P as m approaches infinity.

In short, the above observation implies that in order to find $\pi(s,t)$ we first need to subdivide appropriate edges of G into smaller segments. A problem with this is that as m increases the number of edges in G_m increases at much faster rate and determining the shortest path in G_m via Dijkstra's algorithm quickly becomes computationally infeasible. Therefore, the number of edges should be kept reasonably small without compromising the ability of finding $\pi(s,t)$. To overcome this difficulty the following proposal is worth pursuing.

Let K_1 be a graph that contains all the edges e and vertices v contained in $\pi^G(s,t)$. Add to K_1 all the vertices w inserted at the mid-points of the edges that correspond to the edges of P and that are incident to v but not to s and t . We also add to K_1 the edges that can be created by connecting w and v and that lie on P . Note that K_1 is a subgraph of G_1 . Similarly we obtain K_2 from $\pi^{K_1}(s,t)$ and in general K_{m+1} from $\pi^{K_m}(s,t)$. We denote this operation with "*" which allows writing $K_{m+1} = K_m^*$. Now we can state that there exists a positive integer N and a real number $\epsilon > 0$ such that $|\pi^{K_m}(s,t) - \pi(s,t)| < \epsilon$ for all $m \geq N$. This is true because K_m is the subgraph of G_m . With this procedure we are able to reduce the amount of computation to obtain $\pi(s,t)$. The following recursive algorithm given in pseudocode brings the desirable result.

Let $f(G)$ denote a function that returns $\pi(s,t)$. Set s,t,ϵ and $MaxSteps$ to appropriate values. Then the definition of $f(G)$ is:

```

Count = 0;
LenPrevPath = 0;
f(G){
    LenCurrentPath =  $\pi^G(s,t)$ ;
    if( |LenCurrentPath - LenPrevPath| <  $\epsilon$  & Count > MaxSteps) return LenCurrentPath;
    LenPrevPath = LenCurrentPath;
    Count = Count + 1;
    return f(G*);
}

```

The above function will converge to $\pi(s,t)$ only if the vertices and edges in $\pi^G(s,t)$ are “sufficiently close” in geometrical sense to $\pi(s,t)$. The situation is similar to that of the Newton-Raphson method converging to a root of an equation that is trying to solve. To improve the likelihood of the function converging to $\pi(s,t)$, instead of starting from initial graph G , one should start from some subsequent graph G_n with $n + 1$ divided edges. Note that the test $Count > MaxSteps$ above is necessary because it is possible that at some instance $|LenCurrentPath - LenPrevPath|$ may evaluate to zero which, however, does not imply that the solution was reached. Therefore, a sufficient subdivision of the initial graph would allow obtaining the shortest path.

A simple example suffices to illustrate the above procedure. Without the loss of generality we will illustrate the algorithm on a planar graph G where the shortest distance between two points is the length of the straight line. In Figure 4, a planar graph is depicted. Let's suppose that we need to find the shortest distance between s and t (nodes 8 and 4). Path $\pi^G(s,t)$ contains node 8,1,2,3 and 4. We then generate K_1 by inserting vertices at locations represented by a dash (2nd step) and find $\pi^{K_1}(s,t)$. Note that not all edges in K_1 are shown to avoid obscuring the figure. We proceed by inserting the new vertices at locations represented by a square in Figure 4 and find $\pi^{K_2}(s,t)$. We continue until there is no improvement in $\pi^{K_m}(s,t)$ for $MaxSteps$. At that point we will have reached the straight line between 8 and 4.

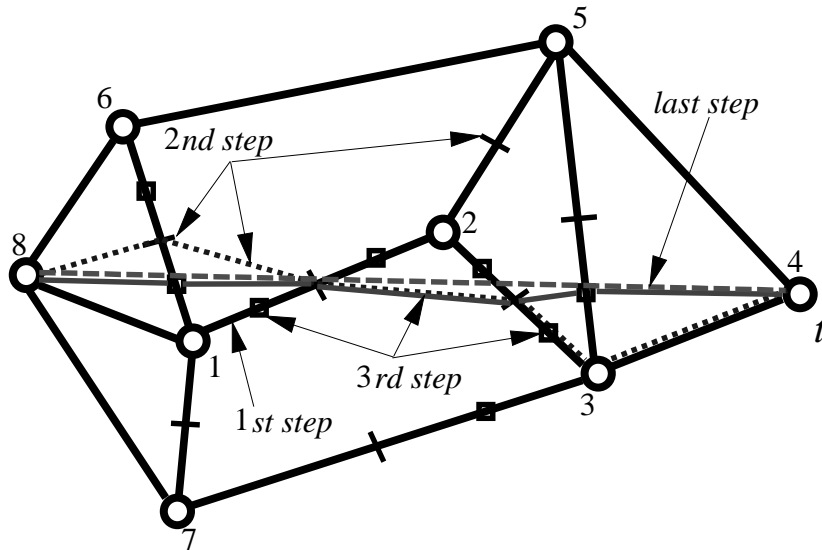


Figure 4. An illustration of the algorithm on a graph in the plane.

5. Weld lines on Polyhedral Surfaces

In this section we consider the construction of Voronoi diagrams on polyhedral surfaces. As explained before, we plan to use the Voronoi concept to approximate weld lines in the RTM process. To achieve this goal we need to be able to subdivide P into regions that satisfy the above proximity assumptions. The development in the previous section will come to our aid here.

Given a set S of n sources on P a Voronoi diagram on P can be defined as follows,

$$vo(p) = \{x \in P : \pi(x, p) \leq \pi(x, q) \forall q \in S - p\} \quad (2)$$

Equation (2) requires a subdivision of P into Voronoi regions. Unfortunately, the available methods for the construction of the Voronoi diagram (Okabe et al, 1992) are not adequate, because they are designed for a set of sites in the plane. In polyhedral spaces one cannot rely on the properties of the plane; however, one simple solution is possible. The idea is to start at a point that belongs to the Voronoi diagram and to walk along the diagram until the boundary for every Voronoi site is determined. As illustrated in Figure 5, this involves traversing the diagram with small circles while at the same time ensuring the appropriate distance between two neighboring sites. For each step a new point that belongs to the Voronoi diagram is located by trying to find an intersection of the circles with the diagram. The final result is a list of stored coordinates that represent the intersections.

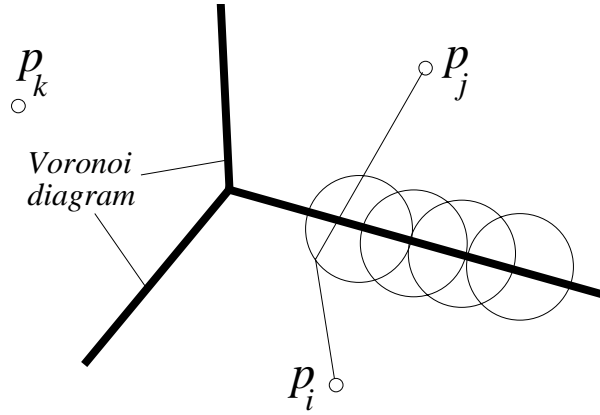


Figure 5. Traversal of the Voronoi diagram.

Note that the boundary of the Voronoi region is a closed curve in 3D space. Stored coordinates are a discretized approximation of the curve. If along the traversal of the region ∂P (boundary of P) is encountered, then the coordinates do not represent the whole boundary of the region and we must repeat the traversal in the areas where the other segments lie. This is however a problem related to the implementation, therefore its solution will not be pursued here.

Once a subdivision of P into Voronoi regions is performed, a reasonable estimate of the weld lines due to resin flow from Voronoi sites on P is available. There might exist, however, some additional weld lines within the Voronoi regions due to their convoluted geometry. This cannot be the case with planar-surface-filling. If there are no inserts present, the resin has only a unique shortest path to traverse to reach a specific point. But, when filling of a region M of P is performed, it is possible to have more than one shortest path from the gate to a point on M . This observation implies that the point might belong to a weld line because having more than two shortest paths to a point is a necessary condition for such an event but not a sufficient one. We will address this issue after we introduce the notion of ridge points.

To explore the consequences of the above observation the following definition is useful. A point $z \in M$ is called a ridge point if there exist at least two shortest paths from a site x to z along M . We denote by R a set of all ridge points on M . Properties of R on polyhedra can be found in Sharir and Schorr, (1986). Assume now that having two shortest paths to a point is also a sufficient condition for the formation of weld lines. Then, from the above observation it follows that we can approximate the weld lines within

Voronoi regions with R . Therefore, we need to determine R on M . To that end, the following characterization is helpful.

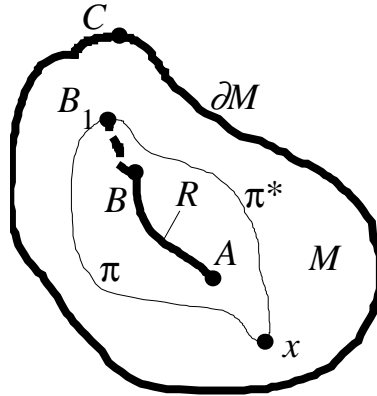


Figure 6. Proof of the lemma.

Lemma: Let R be a set of ridge points on a Voronoi region M , then $R \cap \partial M \neq \emptyset$.

Proof: Suppose there exist a segment $\underline{AB} \in R$ that does not have an intersection with ∂M (Figure 6). Assume that B is further from x than A is. In the vicinity of B there exists at least one point B_1 that can be reached by two different paths from either side of \underline{AB} . For the two equal shortest paths π and π^* , B_1 will be a ridge point. Since the set R is closed and connected (Sharir and Schorr, 1986) there must be other ridge points between B_1 and B that belong to some curve $\underline{BB_1}$. Then the segment $\underline{BB_1} \in R$ holds true as well. By picking another point B_2 in the vicinity of B_1 we can draw a similar conclusion about the segment $\underline{B_1B_2}$. Eventually we will reach a point C on ∂M and determine that $\underline{CB_n} \in R$ implying that the original hypothesis was wrong which proves the lemma. •

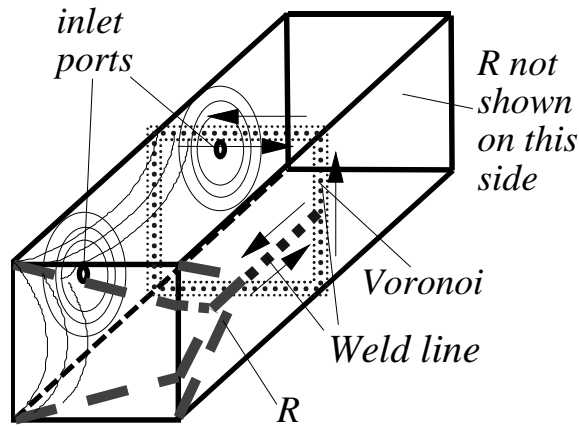


Figure 7. Ridge points on the surfaces of a polyhedron.

As an illustration of the lemma a simple polyhedral object is shown in Figure 7. The object does not have any practical purpose except to demonstrate the concept of ridge points. The gating is done through two gates on the side. The Voronoi labeled line is due to two sites on the object while the dashed R labeled line is due to the left site only. R is determined by using the lemma. Therefore a

starting point for the location of R is sought along the parts of the Voronoi diagram that belong to the site in question.

We assumed above that having more than two shortest paths to a point is a sufficient condition for the formation of weld lines. However, in general this is not the case and we have to address the situation when weld lines do not form even though the fluid is able to flow to a particular regions from at least two different directions. Let us examine the situation where such a case might arise. First, we define R^* to be a set that contains R and all vertices of P that are infinitely close to any point of R . Then R^* is a tree having (some of) the vertices of P as leaves. In Figure 8 a case where such a leaf will arise that may or may not represent a weld line is depicted.

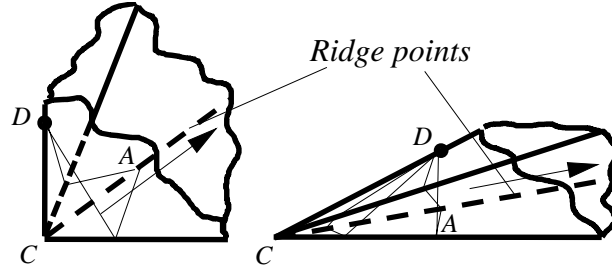


Figure 8. Development of weld lines around a corner.

Point D is the inlet port. Point C is the last point on the leaf of the tree for source D . Point A is a point on the leaf that can be reached from the source. On the corner to the left in Figure 8 the shortest path from D to C is smaller than that from D to A measured along the surface of the body while on the corner to the right it is the opposite case. On the left corner the resin flowing from D reaches C before A , while on the right corner it reaches point A first. This means that the weld line will be formed only on the body to the right in Figure 8. In fact, it can be inferred that if the length of the shortest path from the source monotonically increases as we traverse from the end of the leaf towards its beginning, the leaf will not turn into a weld-line and it should be discarded from further analysis.

The presence of inserts in the mold results in formation of additional weld-lines. In such cases the determination of the vents should be performed as described in Biccard et al, (1995).

Once a determination of the weld lines is done, one can proceed with determination of vent locations. Vents should be located at the maximum of the r versus s curve where r is the shortest path between the inlet port and a position s along the closed curve generated by traversing the weld lines and the boundary of the object. Observe the traversing direction implied by the arrows in Figure 7. The Voronoi region together with R can be visualized as a disk distorted in such a way that some parts of its boundary merged to form R .

6. Mold Filling Time Estimates

Estimating the mold filling time is another very important factor in the analysis of the RTM process. This proves to be the most difficult task in the simplified approach due to the fact that so many variables play significant roles in mold filling time calculation.

We assume that one has been successful in subdividing the whole body into Voronoi regions as it was described above. Now, it is necessary to determine the mold filling time for each inlet port that fills its

own region. The maximum time of all the times for each inlet port is an estimate of the time to fill the mold. Therefore, one needs to be able to determine the filling time of one Voronoi region with only one inlet port. We start with a simple observation that the Voronoi region is completely filled when the resin front reaches the vent which is the furthest from the inlet port in that region. Therefore, the maximum distance to the vent dictates the required time for the resin to reach the vent.

In Biccard et al, (1995) a simplified procedure was proposed to estimate the mold filling time. It was based on the following reasoning. In the vicinity of the inlet port, the resin flows in a radial manner, while near the boundary of the mold the resin flows along the boundary and resembles the flow in a channel. Therefore, the authors assumed that the actual resin flow is the combination of the two. They used the filling time formulae developed in Cai, Z. (1992),

$$t_{fill}^R = M \left(\frac{r_f}{r_o} \right)^2 \left\{ 2 \ln \left(\frac{r_f}{r_o} \right) + \left(\frac{r_o}{r_f} \right)^2 - 1 \right\} \quad (3)$$

$$t_{fill}^C = 2M \left(\frac{r_f}{r_o} - 1 \right)^2 \quad M = \frac{\mu \varepsilon r_o^2}{4 K p_o}$$

where μ is the viscosity of the resin, ε is the porosity of the preform, p_o is the injection pressure at the inlet port, r_o is the radius of the inlet port, r_f is the maximum shortest distance from the center of the inlet port and K is the permeability of the preform. Equation (3) is for the case when the mold is filled with the fibrous preform.

The filling time t_{fill}^R for the radial flow and the filling time t_{fill}^C for the channel flow were linearly interpolated to find the filling time t_{fill} of the region, $t_{fill} = \beta t_{fill}^R + (1 - \beta) t_{fill}^C$. The interpolation factor β for a Voronoi region with an inlet port P is determined through a geometrical construction proposed in Biccard et al, (1995). The factor represents the percentage of available flow space for a particular geometry relative to the flow space that the resin would have been able to occupy if it were to flow only radially. The calculation involves determining the relevant areas with use of tangential points on the perimeter closest to P . Unfortunately, such construction in polyhedral spaces often does not yield meaningful results and it cannot be implemented without extensive computational effort. Nevertheless, the interpolation idea is appealing and it is possible to devise a different line of reasoning to determine β whose construction is independent of the dimensionality of the flow space

Following the assumption that the resin will flow through the region F along the shortest paths to reach the furthest points, we can attempt to determine β by calculating the perimeter of the flow front. The assumption implies a simplification that all the points of the flow front will be at the same increasing shortest distance from the inlet port. As it is being injected at gate G , the resin will flow through the available flow space. The perimeter of the flow front will then be subjected to contraction or expansion until the resin reaches the last point at distance R_{max} . For a general shape of the mold (left object in Figure 9), the perimeter will reach a maximum value L at some shortest distance R from the gate. If the resin had been free to flow through the perimeter L without any constraints, its covered area

would have exactly resembled the segment C of the circle with radius R_{max} and angle ϕ corresponding to arc length L at radius R (right object in Figure 9). However, since the resin is forced to flow through a region with convoluted boundaries this is not the case. Therefore, the area C_r of available shortest paths through L towards the boundary is smaller than that of C . The ratio of these two areas determines factor β which represents the measure of imposed constraint on the resin. Therefore, $\beta=1$ (radial-like flow) is the case with no constraint, while $\beta=0$ (channel-like flow) is the case with the maximum constraint. Note that there may be several equivalent maximum values of L for a particular geometry. In that case the relevant R will be one that corresponds to L which represents the flow front closest to the gate.

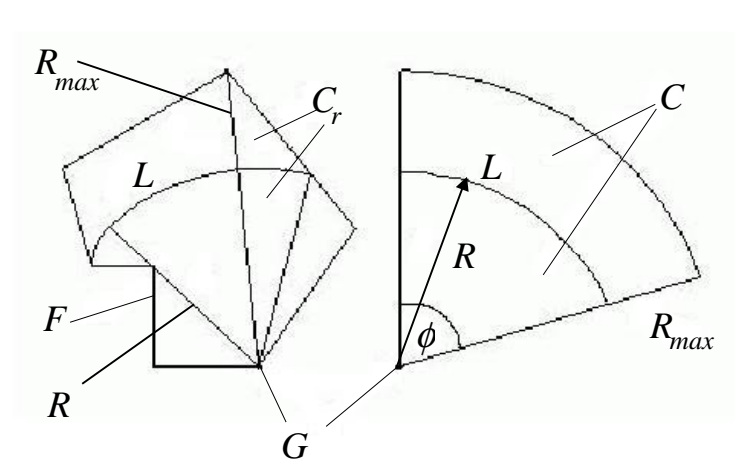


Figure 9. Determination of the beta factor.

To facilitate the implementation a more precise mathematical statement of the above is provided in Equation (4). The flow fronts of the polymer are the level curves described as follows:

$$M(c) = \{p \in F : \pi(G, p) = c\} \tag{4}$$

$$L = \max_{\min c} M(c)$$

where L corresponds to the maximum arc length which is the maximum of $M(c)$. If there are many equivalent L 's for different c 's, then that L which corresponds to minimal c is the chosen one.

In summary, the determination of the β factor, as described above, has two main advantages. It enables one to determine β for general thin sections and prevents irregularities at the boundary (rapid change of curvature) to influence β . The significance of the latter is best appreciated if one attempts to determine the factor, as proposed in Biccard et al, (1995), for a shape with an erratic boundary. In that case the construction results in β which produces large filling time errors.

Finally, it is interesting to observe that the contraction of the flow space at the corners does not affect the filling injection time. This observation provides means for reducing the computational effort by excluding the areas at corners as demonstrated in Figure 10. The object shown is being filled at gate G . The vent locations are determined to be at V_1, V_2 and V_3 . The furthest vent is at V_2 determined by the

longest of the shortest paths $GA V_2$ or $GB V_2$. The area $GA V_2 B$ associated with corner C does not add to the filling time due to the fact that it takes the same amount of time to fill the object with or without the area.

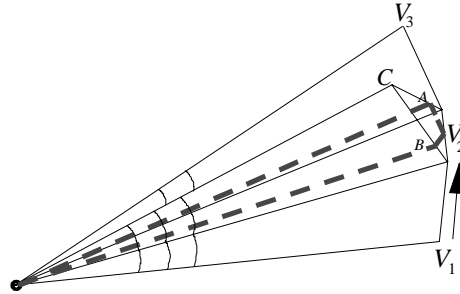


Figure 10. Contraction of the flow space at corners.

7. Illustrative Examples

In this section we present a few RTM examples. The examples were not chosen to prove or disprove the above exposition, but rather to illustrate the application of the proposed concept. Certainly a wider scope experimental study is needed similar to one provided in Biccard et al, (1995).

The first example is simple enough to be evaluated without the assistance of a computer program and it is a good demonstration of the concepts discussed in the previous sections. It is required to estimate weld lines, vent arrangements and the fill time for a hollow box of size 160 x 80 x 30 mm and a thickness of 5 mm which is to be filled through three inlet ports of 1 mm radius arranged as depicted in Figure 11. The distance between gates A and C is 160 mm while gate B is at the mid point of one of the bottom edges of the box.

To obtain the required estimates the first step is to determine the Voronoi diagram for the given object and given sites. The easiest way to manually perform such a procedure is to unfold the surfaces of the box along the appropriate edges. In Figure 11 the result of the analysis is shown. The approximate location of the weld lines are determined by the location of the Voronoi diagram (heavy solid lines) and ridge points (dashed lines). In this case only the Voronoi diagram alone represents the required estimate of weld lines. The ridge points are not taken into consideration according to the observation from the previous section.

Once the estimate of the weld lines is obtained, we proceed with estimating the vent locations. This is done by performing the traversal along the estimated lines for each Voronoi region and labeling all the locations that represent the maximum of distance vs. perimeter curve. Note that some vent locations will not be viewed as vents relative to both neighboring regions as is the case with V_3 and V_5 . Nevertheless, this should be a general rule, even if only one region estimates a vent location, that is a valid estimate and must be included.

For comparison purposes a result from a simulation of the problem done on a commercially available package C-MOLD based on finite element analysis is also shown. The weld lines (wider bands across) seem to be in good agreement with the predicted lines as well as the location of vents. Observe that the

air entrapments (crosses in the figure) produced by C-MOLD are not symmetrically distributed even though the inlet ports are symmetric relative to the mid points of the longest sides of the box. This indicates nonuniform meshing generated by C-MOLD. The model in Figure 12 is however free of these problems and it correctly estimates a vent location at V_3 . This indicates usefulness of the proposed model in providing more insight where the more sophisticated and time consuming FEM related analyses may not necessarily reveal more accurate prediction.

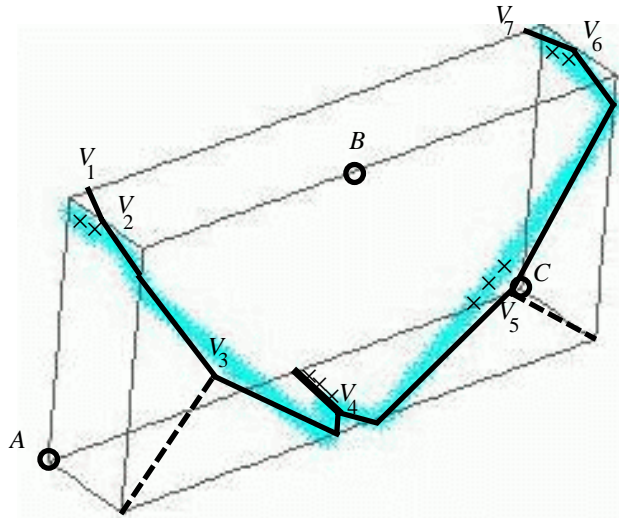


Figure 11. Result of the analysis for the box.

The final step that remains is the calculation of the filling time. According to the exposition from the previous section there are two distinct Voronoi regions for which the filling time must be calculated; the regions attributed to gate B and A (or C). An appropriate geometrical construction was carried out and it was determined that for the inlet ports of radii $r_0=1$ mm, maximum shortest distance from the gates to the estimated weld lines $r_f=84$ mm, permeability $K=8 \cdot 10^{-10} \text{ m}^2$, porosity $\epsilon=.6$, viscosity $\mu=1 \text{ Pa s}$ and the constant pressure $p_0=1 \text{ MPa}$ at the inlet ports, the filling time should be 8.67 s for the region of gate B ($\beta=.77$) and 8.78 s for the region of gate A (or C , $\beta=.79$). These results are in reasonable agreement with that of 7.2 s generated by C-MOLD.

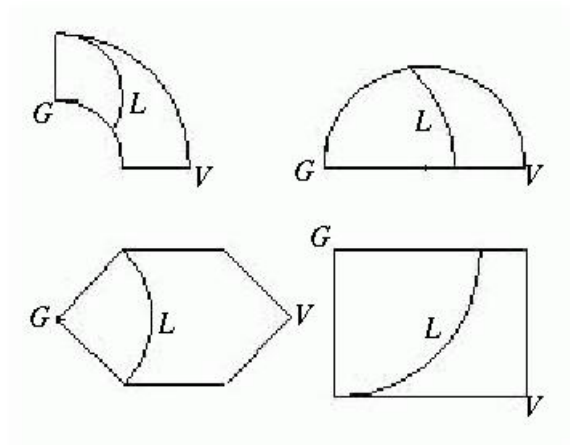


Figure 12. Four selected shape from Biccard et al, (1995).

The next set of examples, shown in Figure 12, is a selection of 2D shapes with distinct geometry and the same input data taken from Biccard et al, (1995). The inner and outer radius of the top left shape are 101.6 mm and 203.2 mm respectively. The radius of the top right shape is 152.4 mm. For the bottom left shape the distance between two horizontal lines and their lengths are 203.2 mm and 152.4 mm respectively, while the distance between G and V is 304.8 mm. The bottom right shape is a rectangle with sides 292.1 mm and 221.7 mm. All the shapes are gated at location G for which the ventilation analysis discussed previously predicted the correct location of vents labeled V . The curve of length L is the first location of the maximum perimeter that the flow attains starting at G . According to our model this is the position of the flow front for which we determine its length. The lengths of the curves and their location produced β and filling time errors relative to the experiment as follows: top left shape $\beta=.45$ ($L=210.4$ mm, $r_f= 229.1$ mm) and -23%, top right shape $\beta=.79$ ($L=171$ mm, $r_f= 304.8$ mm) and 23%, bottom left shape $\beta=.54$ and -8%, and bottom right shape $\beta=.59$ and 0%. The β factors and filling time errors are close to those presented in Biccard et al, (1995) which are as follows: top left shape $\beta=.48$ and -17%, top right shape $\beta=.80$ and 26%, bottom left shape $\beta=.54$ and -8%, and bottom right shape $\beta=.59$ and 0%

Our final example is a part (selected from our own database of automotive parts) shown in Figure 13 with its most important dimensions shown in millimeters. The parts thickness is 5 mm and is gated at location G with the radius of 1 mm. The processing and material input data are the same as in our first example. To obtain a representation of a polyhedral object, the curved mid-surface of the part was mashed and triangulated with ProEngineer using an appropriate finite element mesh size.

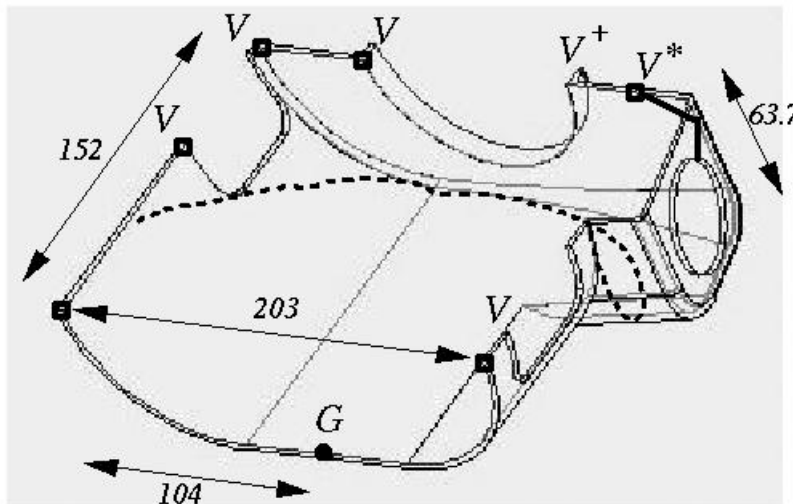


Figure 13. An RTM example (steering shroud).

Our model estimated the locations of the vents V which closely match those predicted by C-MOLD shown as dark squares. However, observe that the first left vent in the front of the part, predicted by C-MOLD, does not correspond to our model estimates. Also, observe one missing dark square under V^+ not predicted by C-MOLD. The left front vent should not be needed, since it was observed in practice that air entrapments at the nearest corners do not materialize when filling rectangular shapes. The left side of the front section can be viewed as a part of a rectangle if it is flattened into a plane. This observation implies that the model can be used by a designer as a checking tool to warn for potential

pitfalls of finite element analysis. The model also estimated a weld line (solid line) due to the insert (circular opening) on the right hand side of the part. The dashed line represents an estimate of the longest flow front of length 366 mm on a distance 152 mm from the gate which gives the angle of 2.4 rad for the maximum possible unobstructed flow. Maximum shortest distance from the gate is 221 mm at the location V^* . Distances were determined by using the algorithm from section 3. The area of the maximum possible space for the unobstructed flow is found to be 58800 mm² as opposed to the 40830 mm² region that is actually available for the resin to go through the maximum perimeter of 366 mm. This determines $\beta = .69$ and results in an estimated filling time of 67 s which is very close to the filling time of 63 s predicted by C-MOLD.

8. Conclusion

In this paper we attempted to characterize a resin flow distribution in parts represented by polyhedral spaces. The purpose of the study was to obtain a model which will, within reasonable accuracy, estimate main RTM parameters such as weld lines, vent locations and filling times. To reach the goal, we utilized the concept of the Voronoi diagram with each inlet port treated as a Voronoi site and the boundary of each Voronoi region as an estimate of weld lines. The boundaries of the regions were determined using a simple shortest path algorithm between two points in polyhedral spaces. Also, we included an analysis related to the concept of ridge points that yielded further insights about the shape of the weld lines. We showed that the length of the flow front can be utilized to estimate the filling times. Estimates obtained for the presented numerical example were in good agreement with more accurate analysis results. However, to obtain a more accurate picture of the usefulness of the proposed model further numerical and empirical studies must be undertaken as well as investigation of RTM in polyhedral spaces not topologically equivalent to a disk. Also, the effect of the mesh size, which determines the size of polyhedral surfaces, should be further investigated in relation to the proposed computational model.

Acknowledgment

The work was supported through a grant made available to the Design and Manufacturing Institute at Stevens Institute of Technology by US Army, Armament Research Development & Engineering Center (Grant No. DAAE30-97-C-1041).

References

- Advani, S., (1994), "*Flow and rheology in polymer composites manufacturing*", Elsevier.
- Antonelli, D., Farina, A., (1999), "Resin transfer molding: mathematical modeling and numerical simulations", *Composites Part A* 30 pp. 1331-1385.
- Aurenhammer, F., (1991), "Voronoi diagrams: A survey of a fundamental data structure," *ACM Comput. Surv.* **23**: 345-405
- Biccard, A., Lee, W., and Springer, G., (1995), "Model for Determining the Vent Locations and the Fill Time of Resin Transfer Molds," *Journal of Composite Materials*, **29**:306-303.
- Cai, Z., (1992), "Analysis of Mold Filling Simulation in Resin Transfer Molding," *Journal of Composite Materials*, **26**:1310-1338.

- Chen, J. and Han, Y., (1996), " Shortest paths on a polyhedron, Part I: Computing shortest paths," *International Journal of Computation Geometry & Applications*, **6**(2): 127-144.
- Deo, N., (1974), *Graph theory with applications to engineering and computer science*, Englewood Cliffs, N.J., Prentice-Hall.
- Dijkstra, E.W., (1959), "A note on two problems in connection with graphs," *Numerische Matematik*, **1**:269-271.
- Fortune, S., (1987), " A sweepline algorithm for Voronoi diagrams," *Algorithmica* **2**: 153-174
- Golestanian, H., El-Gizawy, A., (1998), "Physical and numerical modeling of mold filling in resin transfer molding", *Polymer Composites*, vol.19, No.4
- Mohan R., Ngo, N., Tamma, K., (1999), "On a pure finite element based methodology for resin transfer filling simulations" *Polymer engineering and science*, vol.20, No.1
- Okabe, A., Boots, B. & Sugihara, K., (1992), *Spatial Tessellations: Concepts and Applications of Voronoi Diagrams*, Wiley, Chichester, England.
- Sharir, M. and Schorr,A., (1986), "On the shortest paths in polyhedral spaces", *SIAM Journal on Computing* **15**:193-215.
- Yalvac, S., A. Cohen and M. Pollard., (1992), "A Review of Molding of Resin Transfer Molding Process-Part 2: Mold Filling Simulations," *Proceedings of the First International Conference on Transport Phenomena in Processing, Honolulu*, Honolulu, Hawaii, March 22-26, 1992, pp. 1194-1202.